DOI: 10.1002/cbic.200700656

How Metal Ions Affect Amyloid Formation: Cu^{2+}- and Zn^{2+}-Sensitive Peptides

Kevin Pagel,[a] Tomomi Seri,[a] Hans von Berlepsch,[b] Jan Griebel,[c] Reinhard Kirmse,[c] Christoph Böttcher,[b] and Beate Koksch*[a]

The common feature of proteins involved in many neurodegenerative diseases is their ability to adopt at least two different stable conformations. The conformational transition that shifts the equilibrium from the functional, mostly partially α-helical structure, to the β-sheet rich amyloid can be triggered by numerous factors, such as mutations in the primary structure or changes in the environment. We present a set of model peptides that, without changes in their primary structure, react in a predictable fashion in the presence of transition metal ions by adopting different conformations and aggregate morphologies. These de novo designed peptides strictly follow the characteristic heptad repeat of the α-helical coiled-coil structural motif. Furthermore, domains that favor β-sheet formation have been incorporated to make the system prone to amyloid formation. As a third feature, histidine residues create sensitivity towards the presence of transition metal ions. CD spectroscopy, ThT fluorescence experiments, and transmission electron microscopy were used to characterize peptide conformation and aggregate morphology in the presence of Cu^{2+} and Zn^{2+}. Furthermore, the binding geometry within peptide–Cu^{2+} complexes was characterized by electron paramagnetic resonance spectroscopy.

Introduction

The formation of insoluble amyloid fibers is a common hallmark of many neurodegenerative diseases, such as Alzheimer's disease, type II diabetes, Parkinson's disease, and the transmissible spongiform encephalopathies.[1,2] Additionally, various nondisease related proteins have recently been shown to aggregate into similar fibrillar structures under in vitro conditions; this suggests that the amyloid structure is a general feature of peptides and proteins.[2,3] Although there are usually no sequence homologies, the molecular architecture within the fibrillar assemblies features impressive similarities.[4,5] More importantly, the soluble forms of amyloid-forming proteins mostly exhibit an unfolded or partially α-helical conformation, while their insoluble, amyloid analogues are rich in β-sheets. Interestingly, proteins that convert to amyloids without extensive structural transitions have also been reported.[6–8] Nevertheless, for most naturally occurring amyloids there is a certain necessity for a conformational transition that, as a consequence, shifts the equilibrium from the native structure to the aggregated amyloid form.[9,10] Many striking factors have been reported to act as a trigger for structural conversions; these range from mutations in the primary structure to changes of the environmental conditions, such as pH, metal ions, protein concentration, and oxidative stress.[11–14] Due to the naturally high concentration of heavy metal ions in the brain and their importance in the context of neurodegenerative diseases, the influence of metallochemical reactions on protein conformation and amyloid formation has especially drawn attention in recent years.[15–17]

Although substantial progress towards the understanding of amyloid formation has been made in the last decade, the elucidation of the molecular interactions that occur during the structural transformation and the subsequent formation of amyloids on a molecular level is still a challenge. The low solubility of amyloid-forming proteins and a mostly poor synthetic accessibility restrict the spectrum of analytical techniques and, thus, complicate a detailed characterization. Therefore, the development of suitable peptide models that can overcome the above-mentioned drawbacks of natural systems is of paramount importance.[18]

We present here a series of de novo designed, coiled-coil based, amyloid-forming model peptides that sensitively react in the presence of Cu^{2+} and Zn^{2+} with changes in their secondary structure. Depending on the position of the coordinating histidine residue, metal-ion complexation was shown to either inhibit or accelerate the amyloid-formation process.

[a] *K. Pagel, T. Seri, Prof. B. Koksch*
Institute for Chemistry and Biochemistry, Freie Universität Berlin
Takustrasse 3, 14195 Berlin (Germany)
Fax: (+49) 30-838-55-644
E-mail: koksch@chemie.fu-berlin.de

[b] *Dr. H. von Berlepsch, Dr. C. Böttcher*
Research Centre for Electron Microscopy, Freie Universität Berlin
Fabeckstrasse 36a, 14195 Berlin (Germany)

[c] *J. Griebel, Prof. R. Kirmse*
Institute of Inorganic Chemistry, Universität Leipzig
Johannisallee 29, 04103 Leipzig (Germany)

Supporting information for this article is available on the WWW under http://www.chembiochem.org or from the author.

Results and Discussion

Peptide design

The approach was to implement features of two distinct folds into a de novo designed amyloid model. In order to mimic a native conformation that is rich in α-helices, we applied a design based on the well known coiled-coil folding motif (Figure 1).[19,20] Due to the extensive structural knowledge of this folding motif, it has been widely used as a source for the generation of amyloid-forming model peptides.[21–25] The α-helical coiled-coil usually consists of two to seven α-helices, which are wound around each other with a slight superhelical twist. The primary structure is characterized by a periodicity of seven residues, the so-called 4–3 heptad repeat, which is commonly denoted $(a\text{-}b\text{-}c\text{-}d\text{-}e\text{-}f\text{-}g)_n$, as shown in Figure 1, in blue. Positions a and d are typically occupied by nonpolar residues that form the first recognition motif by hydrophobic core packing. Charged amino acids at positions e and g form the second recognition motif by interhelical ionic interactions. In the case of the model peptides presented here, positions a and d are exclusively occupied by leucine residues; this ensures an efficiently packed hydrophobic core. Positions e and g were designed to form exclusively attractive electrostatic interactions between the helices in case of parallel folding (Figure 1 A, frame).

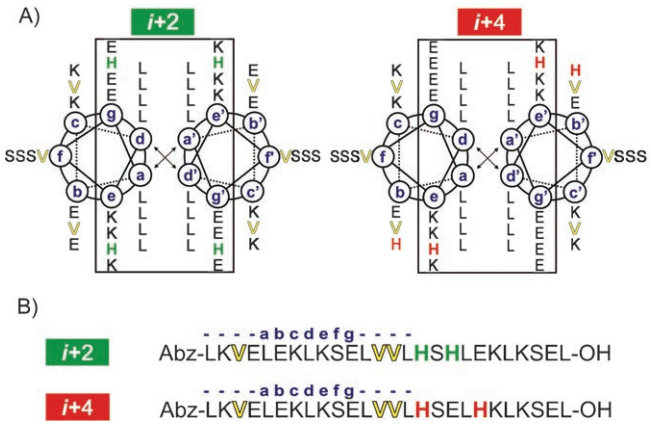

Figure 1. A) Helical wheel diagram, and B) sequence of peptides *i*+2 and *i*+4. The design contains three features: I) intact coiled-coil interaction domains (frame), II) valine at the b, c, and f position to generate an intrinsic amyloid-formation propensity (yellow), and III) metal-binding His to disrupt (green) or induce (red) the helical structure upon metal coordination.

In contrast, positions b, c, and f are solvent exposed (Figure 1 A). As these positions only have a minor impact on coiled-coil stability, introduction of modifications will not affect both helix-forming recognition motifs. Previous studies by our group have shown that incorporation of three β-sheet preferring valine residues at the b, c, and f positions of the heptad repeat sufficiently enhance the amyloid-formation propensity of a 26-residue coiled-coil peptide.[24,26] Thus, three valine residues were incorporated into the model peptides presented here to yield an inherent competition between α-helical coiled-coil folding and the β-sheet rich amyloid structure.

Since it was our aim to design amyloid-forming models that react in the presence of transition metal ions, His residues were incorporated as a key feature (Figure 1). Different strategies for the design of metal-ion sensitive functionalities have been reported; these range from the mimicry of naturally occurring zinc-finger patterns to de novo approaches.[12,27–29] We followed the *i*+2 and *i*+4 strategy which has already been utilized for the characterization of the effects of Fe^{III} binding by non-natural ligands.[28] Incorporation of His at *i* and *i*+2 positions within the *heptad* repeat led to a strong distortion of the peptide backbone upon metal binding, and resulted in destabilization of the helical structure and subsequent unfolding. Incorporation of His at positions *i* and *i*+4 yielded a contrary behavior. Here, both residues are in close spatial proximity in case of helical folding. Therefore, metal coordination results in stabilization of the helical conformation.[28]

Structural characterization

The time-dependent amyloid formation of peptides *i*+2 and *i*+4 was followed by circular dichroism (CD) spectroscopy and Thioflavin T (ThT) staining experiments. Furthermore, transmission electron microscopy (TEM) was applied for the characterization the resulting aggregates.

Starting with a partially helical conformation, peptide *i*+2 slowly formed amyloids within 120 h in the absence of metal ions, as indicated by the appearance of one minima at 216 nm in the CD spectrum (Figure 2 A). As expected, incubation with two equivalents of Cu^{2+} yielded an unfolded conformation, with one prominent minimum at 200 nm, which was retained for the entire observation period of ten days (Figure 2 B). In contrast to our expectations, addition of two equivalents of Zn^{2+} did not lead to unfolding but rather resulted in the acceleration of amyloid formation. The β-sheet conformation was detected by CD spectroscopy within the first 100 h (Figure 2 C).

The ThT-staining assay confirmed the observed differences between Cu^{2+} and Zn^{2+} (Figure 3 A). Without metal addition, a sigmoidal increase of the dye's fluorescence intensity was observed; this points to the typical pathway of nucleation-dependent amyloid elongation. Not surprisingly, Cu^{2+} addition yielded almost unchanged fluorescence intensities, which supports the CD spectroscopic observations of a random-coil conformation. As already assumed from the CD spectra, addition of Zn^{2+} led to accelerated amyloid formation, as indicated by a rapid increase in ThT fluorescence intensity. In order to clarify the different amyloid formation tendencies observed by spectroscopy, the resulting peptide aggregates were characterized by negative-staining TEM after incubation for seven days. In the absence of metal ions, peptide *i*+2 formed fibrils with either long straight and/or flexible ribbon morphology (Figure 3 B and Supporting Information). In contrast, in the presence of Cu^{2+}, aggregates possessed an amorphous morphology; this emphasizes the occurrence of unfolded species (Figure 3 C). Consistent with the spectroscopic data, Zn^{2+} addition yielded

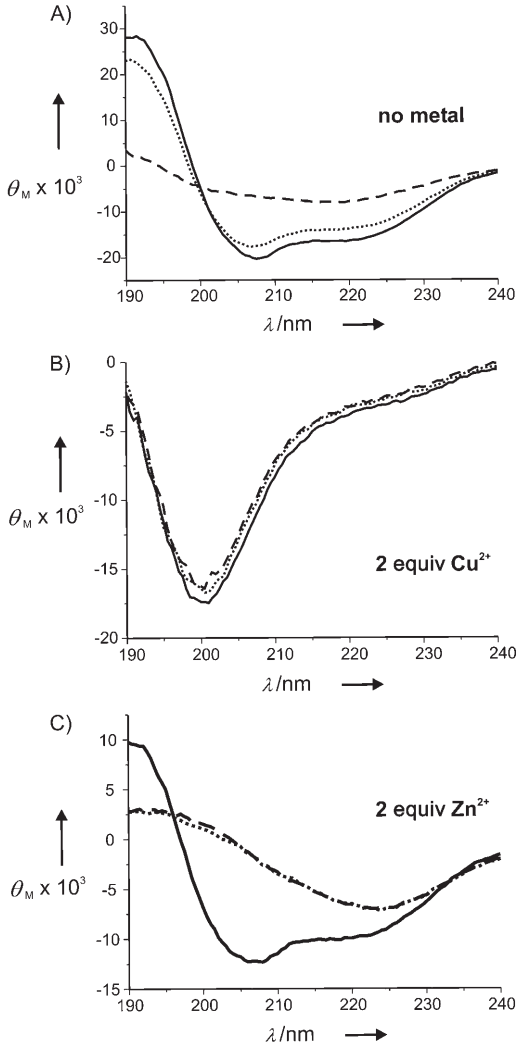

Figure 2. CD spectra of peptide *i*+2: A) without metal ions, B) in the presence of 2 equiv Cu^{2+}, or C) in the presence of 2 equiv Zn^{2+}. Spectra were recorded after 6 h (——), 96 h (····), and 120 h (-----); 100 μM peptide, 200 μM $Cu(OAc)_2$ or $Zn(OAc)_2$, 10 mM phosphate buffer pH 7.4.

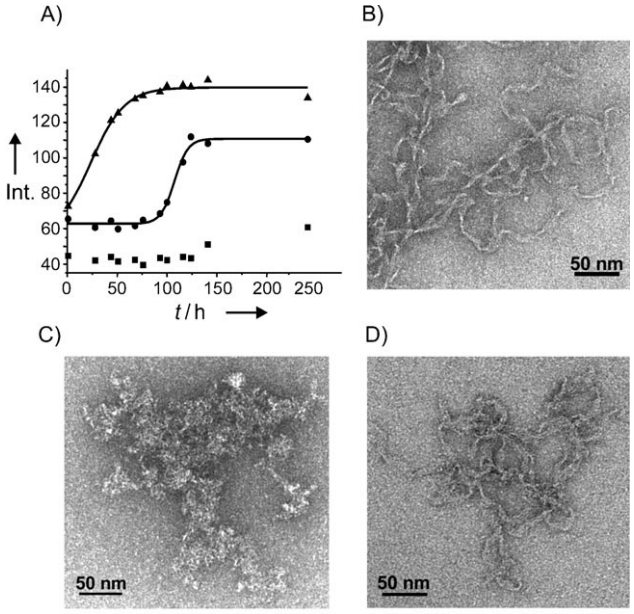

Figure 3. A) ThT-staining assay of peptide *i*+2 in the absence of metal ions (●), and in the presence of 2 equiv Cu^{2+} (■) or Zn^{2+} (▲); 50 μM peptide, 50 μM ThT, 100 μM $Cu(OAc)_2$ or $Zn(OAc)_2$, 10 mM phosphate buffer, pH 7.4. Negative staining transmission electron micrographs (TEM) of peptide *i*+2: B) in the absence of metal ions, C) in the presence of 2 equiv Cu^{2+}, and D) in the presence of 2 equiv Zn^{2+}; 100 μM peptide, 200 μM $Cu(OAc)_2$ or $Zn(OAc)_2$, 10 mM phosphate buffer pH 7.4, 7 days incubation.

ribbon-like amyloid fibers similar to those observed in the absence of metal ions (Figure 3 D).

In contrast to *i*+2, peptide *i*+4 did not discriminate in secondary-structure formation upon coordination to either Cu^{2+} or Zn^{2+}. In the absence of metal ions peptide *i*+4 rapidly converted from a mainly unfolded state to a β-sheet; this indicates fast amyloid formation (Figure 4 A). Addition of either Cu^{2+} or Zn^{2+} yielded helical structures that were retained for the entire observation period of ten days (Figure 4 B and C). Staining of the resulting aggregates with ThT confirmed the CD data. Without metal addition a strong increase in the dye's fluorescence was observed, while samples incubated with either Cu^{2+} or Zn^{2+} did not show any increase in fluorescence intensity (Figure 5 A). Thus, addition of metal ions to peptide *i*+4 shifted the equilibrium to the helical conformation and, as a result, inhibited the amyloid-formation process.

Furthermore, TEM analysis of the resulting aggregates after seven days of incubation revealed distinct morphological differences. In the absence of metal ions, peptide *i*+4 typically formed twisted fibrils that contained four or more protofilaments (Figure 5 B). Additionally, twisted ribbons and tubular assemblies were found under these conditions (Supporting Information). These results support the spectroscopic observations of a classical amyloid-formation process. In contrast, samples incubated with Cu^{2+} as well as Zn^{2+} did not show aggregates with a fibrous morphology as would be expected for amyloids. In the presence of Cu^{2+}, short and sticky rod-like assemblies were found while the addition of Zn^{2+} yielded cloggy bundles of bended rods (Figure 5 C and D). Although peptide *i*+4 exhibited a similar α-helical CD signature and nonamyloidogenic behavior in the presence of Cu^{2+} and Zn^{2+}, the resulting aggregates were distinctly different. These morphological differences are certainly a result of the different coordination geometry within the peptide–Cu^{2+} and peptide–Zn^{2+} complexes.

On basis of the applied design principles and the observed conformational differences between both peptides it is obvious that the unexpectedly accelerated amyloid formation of peptide *i*+2 in the presence of Zn^{2+} results from both the positioning of the His residues as well as the intrinsic binding characteristics of Zn^{2+}. Extended β-strands in general possess a zigzag alignment. As a result, the His residues at *i* and *i*+2 positions are in close proximity to each other on the same side of the strand, and can therefore be easily accessed by metal ions. His residues at *i* and *i*+4 positions are on the same side of the β-strand. However, His side chains are now located far apart from each other; this prevents efficient metal coordination. Therefore, it appears likely that only metal binding to resi-

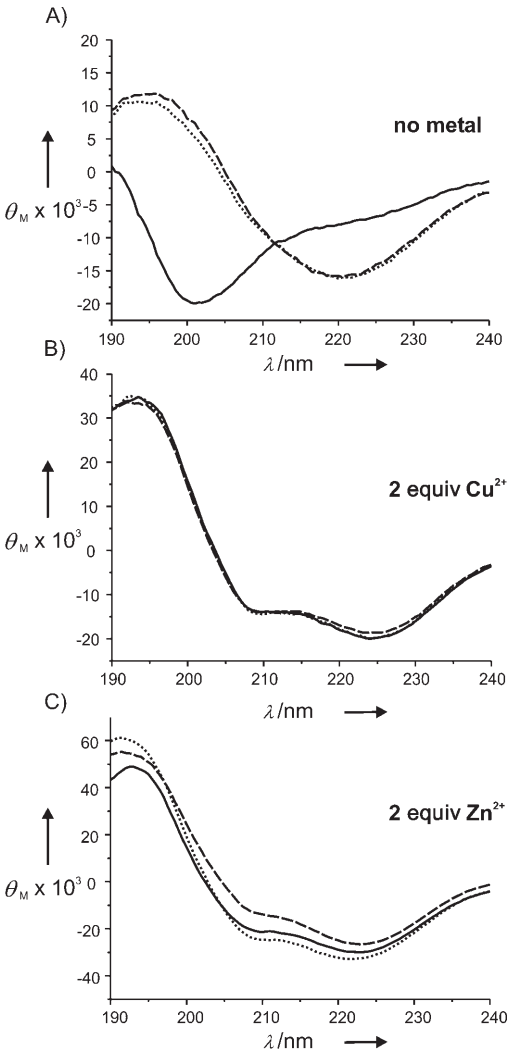

Figure 4. CD spectra of peptide *i*+4: A) without metal ions, B) in the presence of 2 equiv Cu^{2+}, or C) in the presence of 2 equiv Zn^{2+}. Spectra were recorded after 6 h (——), 96 h (····), and 120 h (-----); 100 μM peptide, 200 μM $Cu(OAc)_2$ or $Zn(OAc)_2$, 10 mM phosphate buffer pH 7.4.

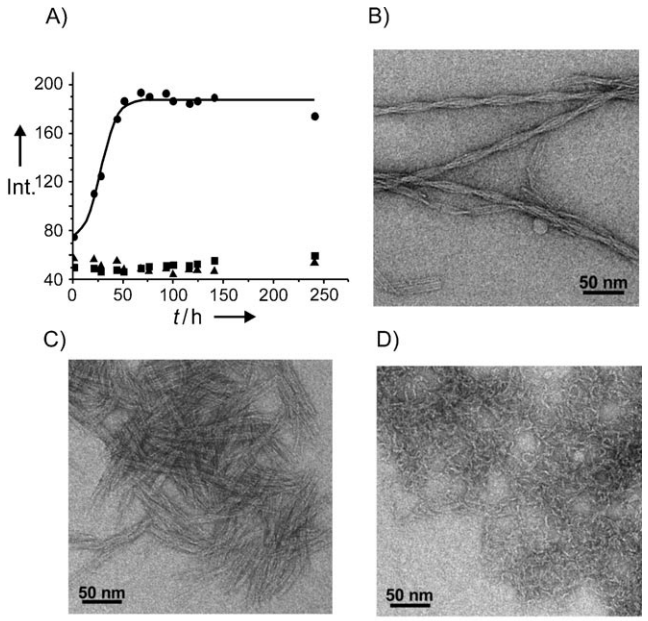

Figure 5. A) ThT-staining assay of peptide *i*+4 without metal ions (●), and in the presence of 2 equiv Cu^{2+} (■) or Zn^{2+} (▲); 50 μM peptide, 50 μM ThT, 100 μM $Cu(OAc)_2$ or $Zn(OAc)_2$, 10 mM phosphate buffer, pH 7.4. Negative staining transmission electron micrographs (TEM) of peptide *i*+4: B) in the absence of metal ions, C) in presence of 2 equiv Cu^{2+}, and D) in presence of 2 equiv Zn^{2+}; 100 μM peptide, 200 μM $Cu(OAc)_2$ or $Zn(OAc)_2$, 10 mM phosphate buffer pH 7.4, 7 days incubation.

dues at positions *i* and *i*+2 has the potential to induce and stabilize amyloids and their β-sheet rich precursors. On the other hand, binding of Cu^{2+} to peptide *i*+2 did not yield accelerated amyloid formation as would be expected from the His positioning. Therefore, the structural preferences of the particular metal ion also seem to significantly affect the amyloid-formation process.

EPR spectroscopy

As assumed from the conformational investigations, differences in the coordination geometry of Cu^{2+} and Zn^{2+} appear to dictate aggregate morphology and the course of amyloid formation. Zn^{2+} usually prefers a coordination number of four with tetrahedral geometry, while most of the cysteine-free Cu^{2+} proteins, the so-called type 2 Cu^{2+} proteins, possess a coordination number of four but with a square planar arrangement.[30–32] A direct determination of the underlying peptide–metal coordination geometry by high resolution methods such as X-ray crystallography is extremely difficult, since amyloid-forming peptides exhibit an extraordinarily high tendency to aggregate, which consequently hampers the growth of crystals. However, the geometry within peptide–Cu^{2+} complexes can be determined sufficiently by using electron paramagnetic resonance (EPR) spectroscopy. Consequently, we performed X-band EPR experiments to shed light on the coordination sphere of the presented peptide–Cu^{2+} complexes and to clarify whether a characteristic type 2 Cu^{2+} center is present.

Figure 6 shows X-band EPR spectra of Cu^{2+} ions bound to peptide *i*+2 and *i*+4. In order to minimize the EPR signal of aqueous Cu^{2+} ions $Cu(OAc)_2$ was used because it forms dimers in frozen solution. The Cu–Cu dimer EPR spectrum is well known,[33] but was not observed in our spectra. Thus, the obtained signal exclusively arose from peptide-bound Cu^{2+}. Both spectra show a typical Cu^{2+} hyperfine splitting with characteristic $g_{\|}$ (the parallel component of the axially symmetric *g* tensor) and $A_{\|}$ (the parallel component of the hyperfine interaction) values; this indicates the presence of a type 2 Cu^{2+} center in a mixed nitrogen/oxygen environment.[34] Similar spectra have been obtained with naturally occurring amyloids, such as Alzheimer's amyloid β (Aβ), α-synuclein, and prion proteins.[35–39] From the obtained values we propose a 2N/2O or 3N/1O coordination environment, since lower $g_{\|}$ and higher $A_{\|}$ values are expected for 4N binding.[35] As a result, it appears likely that at least one His residue within each peptide strand binds to Cu^{2+}, and forms a complex with an almost square

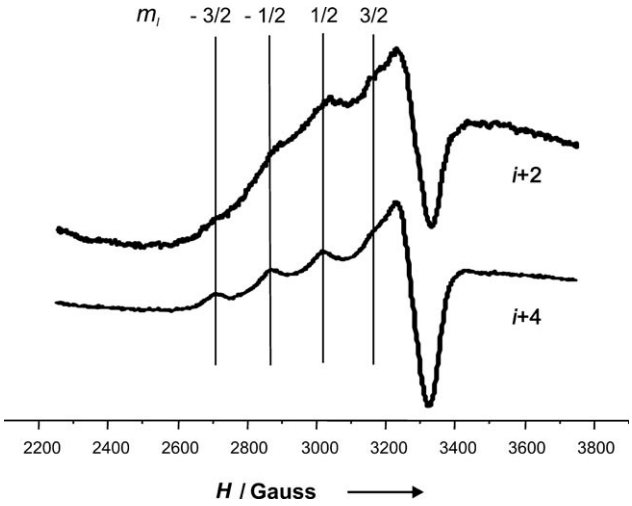

Figure 6. X-band EPR spectra of freshly prepared peptide–Cu^{2+} complexes. Spectra were recorded with 1 mM peptide, 2 mM $Cu(OAc)_2$, 10 mM phosphate buffer pH 7.4, 10% glycerol (*v/v*), $T = 130$ K. *i*+2: $g_\parallel = 2.272$, $A_\parallel = 154\times10^{-4}$ cm^{-1}, $g_\perp = 2.060$; *i*+4: $g_\parallel = 2.284$, $A_\parallel = 158\times10^{-4}$ cm^{-1}, $g_\perp = 2.063$; experimental errors: $g_\perp \pm 0.003$, $A_\parallel \pm 3\times10^{-4}$ cm^{-1}.

planar geometry. ^{14}N hyperfine splittings, which would be helpful for interpretation, could not be resolved.

Since EPR spectroscopy requires unpaired electrons at the metal center it cannot be applied for the characterization of peptide-bound Zn^{2+}. Although a distinct coordination geometry between the peptide–Cu^{2+} and peptide–Zn^{2+} complexes appears obvious from the observed folding behavior and aggregate morphologies, we have not been able to prove these differences yet. Further experiments with sophisticated X-ray absorption near edge structure (XANES) spectroscopy and extended X-ray absorption fine structure (EXAFS) spectroscopy are in progress and might help to formulate a deeper structural understanding.

Conclusions

Based on a de novo design approach, our data clearly highlight the paramount impact of transition metal ion coordination on protein structure and amyloid formation. In the absence of metal ions, both model peptides form amyloids within days. Regardless of the His positions, coordination of Cu^{2+} throughout inhibits the formation of amyloids by either metal-directed unfolding (peptide *i*+2) or helix stabilization (peptide *i*+4). In contrast, the presence of Zn^{2+} was shown to accelerate amyloid formation if two metal-binding sites were placed one residue apart from each other (peptide *i*+2) pointing to the opposite side of the helical cylinder. Zn^{2+} binding to peptide *i*+4, in which the two metal-binding residues are adjacent to each other at the helical cylinder, shows a similar amyloid-inhibiting and helix-inducing behavior as observed for Cu^{2+}. Thus, it can be concluded that metal binding causes inhibition or acceleration of the amyloid-formation process by stabilization or destabilization of a competitive conformation.

In a more general context, our results indicate that not only the position of the coordinating residue but also the nature of the metal ion involved significantly contributes to the amyloid-formation process. The behavior of peptide *i*+2 impressively resembles the Cu^{2+}- and Zn^{2+}-dependent amyloidogenesis of Alzheimer's Aβ in vitro. Recently, Saxena and co-workers[37] showed that the binding of high concentrations of Cu^{2+} to Aβ yields granular nonamyloidogenic aggregates, while Lynn and co-workers[40] reported the accelerating effect of Zn^{2+} binding on the amyloid-formation process. Moreover, Stellato et al. determined perceptible differences in the stoichiometry and coordination geometry of $A\beta_{1-40}$–Cu^{2+} and -Zn^{2+} complexes obtained from resuspended fibrils.[41] Model peptide *i*+2 is a completely artificial, de novo designed molecule and does not possess any sequence homologies to Aβ, even in terms of the His positions. However, it shows a similar folding behavior with inhibition of amyloid formation in the presence of Cu^{2+} and an accelerated amyloid association in the presence of Zn^{2+}. Due to these striking similarities it appears obvious that the intrinsic binding characteristic of the particular metal ion has a bigger impact on amyloid formation than acknowledged so far.

Finally, we can conclude from our experiments that a delicate balance between the position of metal-binding residues and the intrinsic coordination characteristics of Cu^{2+} and Zn^{2+} influences the course of amyloid formation of both presented model peptides. This highly sensitive model system might help to understand molecular details of the transition metal ion dependent amyloid-formation processes.

Experimental Section

Peptide synthesis and purification: Peptides were synthesized by standard Fmoc chemistry by using a Multi-Syntech Syro XP peptide synthesizer (MultiSynTech GmbH, Witten, Germany) with Fmoc-Leu-OWang resin (0.65 mmol g^{-1}). Peptides were N-terminally labeled with anthranilic acid (Abz) to enable photometric concentration determination. Cleavage from the resin was carried out by treatment with 4 mL of a solution containing triisopropylsilane (10%, *w/v*), water (1%, *w/v*), and TFA (89%, *w/v*). Crude peptides were purified by reversed-phase HPLC by using a Knauer Smartline manager 5000 system (Knauer GmbH, Berlin, Germany) equipped with a C8 (10 μm) Phenomenex® LUNA™ column (Phenomenex Inc., Torrance, CA, USA). Peptides were eluted with a linear gradient of water/acetonitrile/0.1% trifluoroacetic acid and identified by ESI-ToF MS. All MS analyses were performed by using an Agilent 6210 ESI-ToF LC–MS spectrometer (Agilent Technologies Inc., Santa Clara, CA, USA) with direct infusion from a Harvard Apparatus 11 Plus syringe pump (Harvard Apparatus, Holliston, MA, USA). Peptide purity was determined by analytical HPLC by using a Merck LaChrom Elite system (Merck KGaA, Darmstadt, Germany) equipped with a C8 (10 μm) Phenomenex LUNA™ column (Phenomenex Inc., Torrance, CA, USA). The applied gradients were similar to those of preparative HPLC.

Sample preparation: Purified peptides were dissolved in freshly prepared and filtered phosphate buffer (10 mM, pH 7.4). Peptide concentration was determined by UV spectroscopy at $\lambda = 320$ nm by using a Varian Cary 50 photometer (Varian Medical Systems, Palo Alto, CA, USA) and PMMA cuvettes (1.5 mL, Plastibrand®, VWR International GmbH, Darmstadt, Germany). Prior to analysis a calibration curve with Abz-Gly-OH (Bachem GmbH, Weil am Rhein,

Germany) in phosphate buffer (10 mM, pH 7.4) was recorded at different concentrations. Subsequently, two equivalents of metal ions were added by using stock solutions (8 mM) of $Cu(Ac)_2$ or $Zn(OAc)_2$ (ACS grade, Acros Organics, Geel, Belgium) dissolved in tridistilled water. Fibrils were formed by incubation at room temperature under stationary conditions.

Circular dichroism: CD spectra were recorded by using a Jasco J-810 spectropolarimeter at 20 °C. Quartz cells (0.1 cm path length) were used throughout. The spectra were the average of three scans obtained by collecting data from 240 to 190 nm at 0.5 nm intervals, 1 nm bandwidth, and 1 s response time. Spectra were background corrected by subtraction of the corresponding buffer spectra. The measured CD data in mdeg were converted into mean residue ellipticity, θ_M.

Thioflavin T assay: ThT (Sigma–Aldrich) was used after purification by reversed-phase column chromatography. Fluorescence spectra were measured by using a luminescence spectrometer LS 50B (Perkin–Elmer, Boston, MA, USA) and a fluorescence cuvette (1.4 mL, 10×2 mm). Samples were prepared by incubating the peptide solution (200 μL, 100 μM, 10 mM phosphate buffer, pH 7.4) that contained the corresponding amount of Cu^{2+} or Zn^{2+} with ThT (200 μL, 100 μM, 10 mM phosphate buffer, pH 7.4) for 30 min. Spectra were measured by accumulating 10 scans from 470 to 600 nm with an excitation wavelength of 450 nm, and background corrected by subtraction of the free-dye spectrum. The given aggregation traces were generated from the ThT fluorescence intensity at 485 nm and were recorded at several time points.

Electron microscopy: Aliquots of peptide solutions (6 μL) were absorbed for 1 min to glow-discharged carbon-coated collodium films on 400 mesh copper grids. After blotting and negative staining with phosphotungstic acid (PTA, 1%) the grids were air dried. TEM micrographs were taken at primary magnification of 58300x by using a defocus of 0.6 μm.

EPR spectroscopy: EPR spectra were recorded by using a Bruker ESP 300E X-band spectrometer (Bruker BioSpin Corp., Billerica, MA, USA).

Acknowledgements

This work was supported by the German Research Foundation (project KO 1976/5-1) and the Freie Universität Berlin. We thank Prof. U. Abram for fruitful discussions.

Keywords: α/β conformational transitions · amyloid fibrils · EPR spectroscopy · peptide–metal binding · protein folding

[1] J. P. Taylor, J. Hardy, K. H. Fischbeck, *Science* **2002**, *296*, 1991–1995.
[2] M. Stefani, C. M. Dobson, *J. Mol. Med.* **2003**, *81*, 678–699.
[3] J. I. Guijarro, M. Sunde, J. A. Jones, I. D. Campell, C. M. Dobson, *Proc. Natl. Acad. Sci. USA* **1998**, *95*, 4224–4228.
[4] R. Nelson, M. R. Sawaya, M. Balbirnie, A. O. Madsen, C. Riekel, R. Grothe, D. Eisenberg, *Nature* **2005**, *435*, 773–778.
[5] O. S. Makin, L. C. Serpell, *FEBS J.* **2005**, *272*, 5950–5961.
[6] I. V. Baskakov, G. Legname, M. A. Baldwin, S. B. Prusiner, F. E. Cohen, *J. Biol. Chem.* **2002**, *277*, 21140–21148.
[7] G. Soldi, F. Bemporad, S. Torrassa, A. Relini, M. Ramazzotti, N. Taddei, F. Chiti, *Biophys. J.* **2005**, *89*, 4234–4244.
[8] G. Plakoutsi, F. Bempord, M. Calamai, N. Taddei, C. M. Dobson, F. Chiti, *J. Mol. Biol.* **2005**, *351*, 910–922.
[9] J.-C. Rochet, P. T. Lansbury, *Curr. Opin. Struct. Biol.* **2000**, *10*, 60–68.
[10] V. N. Uversky, A. L. Fink, *Biochim. Biophys. Acta* **2004**, *1698*, 131–153.
[11] A. Aggeli, M. Bell, L. M. Carrick, C. W. G. Fishwick, R. Harding, P. J. Mawer, S. E. Radford, A. E. Strong, N. Boden, *J. Am. Chem. Soc.* **2003**, *125*, 9619–9628.
[12] E. Cerasoli, B. K. Sharpe, D. N. Woolfson, *J. Am. Chem. Soc.* **2005**, *127*, 15008–15009.
[13] K. Pagel, T. Vagt, B. Koksch, *Org. Biomol. Chem.* **2005**, *3*, 3843–3850.
[14] S. J. Siegel, J. Bieschke, E. T. Powers, J. W. Kelly, *Biochemistry* **2007**, *46*, 1503–1510.
[15] A. I. Bush, *Curr. Opin. Chem. Biol.* **2000**, *4*, 184–191.
[16] A. I. Bush, C. L. Masters, R. E. Tanzi, *Proc. Natl. Acad. Sci. USA* **2003**, *100*, 11193–11194.
[17] K. Pagel, T. Vagt, T. Kohajda, B. Koksch, *Org. Biomol. Chem.* **2005**, *3*, 2500–2502.
[18] M. T. Pastor, A. Esteras-Chopo, M. L. de La Paz, *Curr. Opin. Struct. Biol.* **2005**, *15*, 57–63.
[19] J. M. Mason, K. M. Arndt, *ChemBioChem* **2004**, *5*, 170–176.
[20] K. Pagel, K. Seeger, B. Seiwert, A. Villa, A. E. Mark, S. Berger, B. Koksch, *Org. Biomol. Chem.* **2005**, *3*, 1189–1194.
[21] Y. Takahashi, A. Ueno, H. Mihara, *ChemBioChem* **2002**, *3*, 637–642.
[22] M. J. Pandya, E. Cerasoli, A. Joseph, R. G. Stoneman, E. Waite, D. N. Woolfson, *J. Am. Chem. Soc.* **2004**, *126*, 17016–17024.
[23] R. A. Kammerer, D. Kostrewa, J. Zurdo, A. Detken, C. García-Echeverría, J. D. Green, S. A. Müller, B. H. Meier, F. K. Winkler, C. M. Dobson, M. O. Steinmetz, *Proc. Natl. Acad. Sci. USA* **2004**, *101*, 4435–4440.
[24] K. Pagel, S. C. Wagner, K. Samedov, H. von Berlepsch, C. Böttcher, B. Koksch, *J. Am. Chem. Soc.* **2006**, *128*, 2196–2197.
[25] H. Dong, J. D. Hartgerink, *Biomacromolecules* **2007**, *8*, 617–623.
[26] S. C. Wagner, R. R. Araghi, K. Pagel, H. von Berlepsch, C. Böttcher, B. Koksch, **2007**; unpublished results.
[27] X. I. Ambroggio, B. Kuhlman, *J. Am. Chem. Soc.* **2006**, *128*, 1154–1161.
[28] S. Futaki, T. Kiwada, Y. Sugiura, *J. Am. Chem. Soc.* **2004**, *126*, 15762–15769.
[29] J. P. Schneider, J. W. Kelly, *J. Am. Chem. Soc.* **1995**, *117*, 2533–2546.
[30] M. Klemba, K. H. Gardner, S. Marino, N. D. Clarke, L. Regan, *Nat. Struct. Biol.* **1995**, *2*, 368–373.
[31] R. R. Roe, Y.-P. Pang, *J. Mol. Model.* **1999**, *5*, 134–140.
[32] R. H. Holm, P. Kennepohl, E. I. Solomon, *Chem. Rev.* **1996**, *96*, 2239–2314.
[33] F. G. Herring, R. C. Thompson, C. F. Schwerdtfeger, *Can. J. Chem.* **1969**, *47*, 555–558.
[34] J. Preisach, W. E. Blumberg, *Arch. Biochem. Biophys.* **1974**, *165*, 691–708.
[35] J. W. Karr, L. J. Kaupp, V. A. Szalai, *J. Am. Chem. Soc.* **2004**, *126*, 13534–13538.
[36] J. W. Karr, H. Akintoye, L. J. Kaupp, V. A. Szalai, *Biochemistry* **2005**, *44*, 5478–5487.
[37] S. Jun, S. Saxena, *Angew. Chem.* **2007**, *119*, 4033–4035; *Angew. Chem. Int. Ed.* **2007**, *46*, 3959–3961.
[38] R. M. Rasia, C. W. Bertoncini, D. Marsh, W. Hoyer, D. Cherny, M. Zweckstetter, C. Griesinger, T. M. Jovin, C. O. Fernandez, *Proc. Natl. Acad. Sci. USA* **2005**, *102*, 4294–4299.
[39] J. H. Viles, F. E. Cohen, S. B. Prusiner, D. B. Goodin, P. E. Wright, H. J. Dyson, *Proc. Natl. Acad. Sci. USA* **1999**, *96*, 2042–2047.
[40] J. Dong, J. E. Shokes, R. A. Scott, D. G. Lynn, *J. Am. Chem. Soc.* **2006**, *128*, 3540–3542.
[41] F. Stellato, G. Menestrina, M. D. Serra, C. Potrich, R. Tomazzolli, W. Meyer-Klaucke, S. Morante, *Eur. Biophys. J.* **2006**, *35*, 340–351.

Received: November 2, 2007
Published online on January 29, 2008

